

## Synthesis, chemical–optical characterization and solvent interaction effect of novel fluorene-chromophores with D–A–D structure

Jesús Rodríguez-Romero<sup>a</sup>, Laura Aparicio-Ixta<sup>b</sup>, Mario Rodríguez<sup>b,\*</sup>, Gabriel Ramos-Ortíz<sup>b</sup>, José Luis Maldonado<sup>b</sup>, Arturo Jiménez-Sánchez<sup>a</sup>, Norberto Farfán<sup>c</sup>, Rosa Santillan<sup>a,\*</sup>

<sup>a</sup>Departamento de Química, Centro de Investigación y de Estudios Avanzados del IPN, 07000, Apdo. Postal. 14-740, México D.F., Mexico

<sup>b</sup>Centro de Investigaciones en Óptica A.P. 1-948, 37000 León, Gto., Mexico

<sup>c</sup>Facultad de Química, Departamento de Química Orgánica, Universidad Nacional Autónoma de México, 04510, México, D.F., Mexico

### ARTICLE INFO

#### Article history:

Received 15 October 2012

Received in revised form

22 December 2012

Accepted 27 December 2012

Available online 17 January 2013

#### Keywords:

Fluorene

Donor–acceptor interactions

Solvatochromism

Intramolecular charge transfer

Two-photon absorption

Organic nanoparticles

### ABSTRACT

The synthesis, chemical characterization and optical studies of three novel fluorene derivatives is reported. These compounds comprise a D–A–D architecture with fluorene moieties as donor groups and fluorenone or benzothiadiazole derivatives as acceptor groups. Theoretical analysis confirmed the existence and the nature of two principal electronic transitions ( $\pi \rightarrow \pi^*$  and intramolecular charge transfer). Spectroscopic studies in solution revealed that the intramolecular charge transfer character, and in turn the two-photon activity i.e., the fluorescence induced by two-photon absorption, is strongly affected by solvent polarity. The influence of specific solvent–solute interactions over emission properties was also studied through Lippert–Mataga plot. Evaluation of the two-photon absorption cross-sections, gave a maximum value of 105 GM ( $1 \text{ GM} = 10^{-50} \text{ cm}^4 \text{ s}$ ) in toluene and a minimum value of 23 GM in THF solutions at 750 nm for the fluorenone derivative, a molecule with poor intramolecular charge transfer character and thus weak two-photon absorption; however the benzothiadiazole derivative, with stronger intramolecular charge transfer transition, produced a maximum value of 1000 GM in THF and a minimum value of 236 GM in methanol. Fluorescence quantum efficiency of these compounds was also affected by the medium, with fluorescence quenching in protic solvents such as methanol due to specific solvent interactions (i.e., hydrogen-bonding). Nevertheless, in a more polar medium such as water, nanoaggregates synthesized from the benzothiadiazole derivative exhibited good two-photon activity, i.e.,  $\sim 500 \text{ GM}$  and fluorescence quantum efficiency of 0.83. Furthermore, these nanoaggregates exhibited more resistance against photodegradation processes than any of the organic solutions tested.

© 2013 Elsevier Ltd. All rights reserved.

### 1. Introduction

The design and synthesis of organic conjugated molecules with efficient Two-Photon Absorption (TPA) properties is an area in full expansion [1,2]. These materials find applications in laser scanning fluorescent microscopy [3], optical limiting [4] three dimensional optical data storage [5] and microfabrication [6]. A great variety of organic chromophores have been prepared to investigate the structure–property relationships that are capable of providing exceptional two-photon absorption cross-sections ( $\delta_{\text{TPA}}$ ) values [1,7,8]. Specially,  $\pi$ -conjugated organic molecules that incorporate

a D–A–D (donor–acceptor–donor) architecture, with Intra-molecular Charge Transfer (ICT) process from the edges to the core of the molecular structure, have shown high TPA response of quadrupolar origin [8–10]. In these molecular systems, parameters like planarity and extended conjugation have been investigated with the aim to improve their ICT character [1], whereas various types of electronic donors (D) are utilized including triarylamine, carbazole, and fluorene derivatives; the commonly used electronic acceptors (A) are benzothiazole, triazine, benzothiadiazole, carbazole, coumarins, porphyrins and fluorene derivatives linked to D by a  $\pi$  bridge [8,11].

A parameter that plays a significant role on the TPA properties exhibited by organic chromophores is the molecular environment; this is because in solutions the dipole moments for ground and excited states are affected by solvent polarity. The effect of solvent polarity on TPA is not well understood yet, although some

\* Corresponding authors.

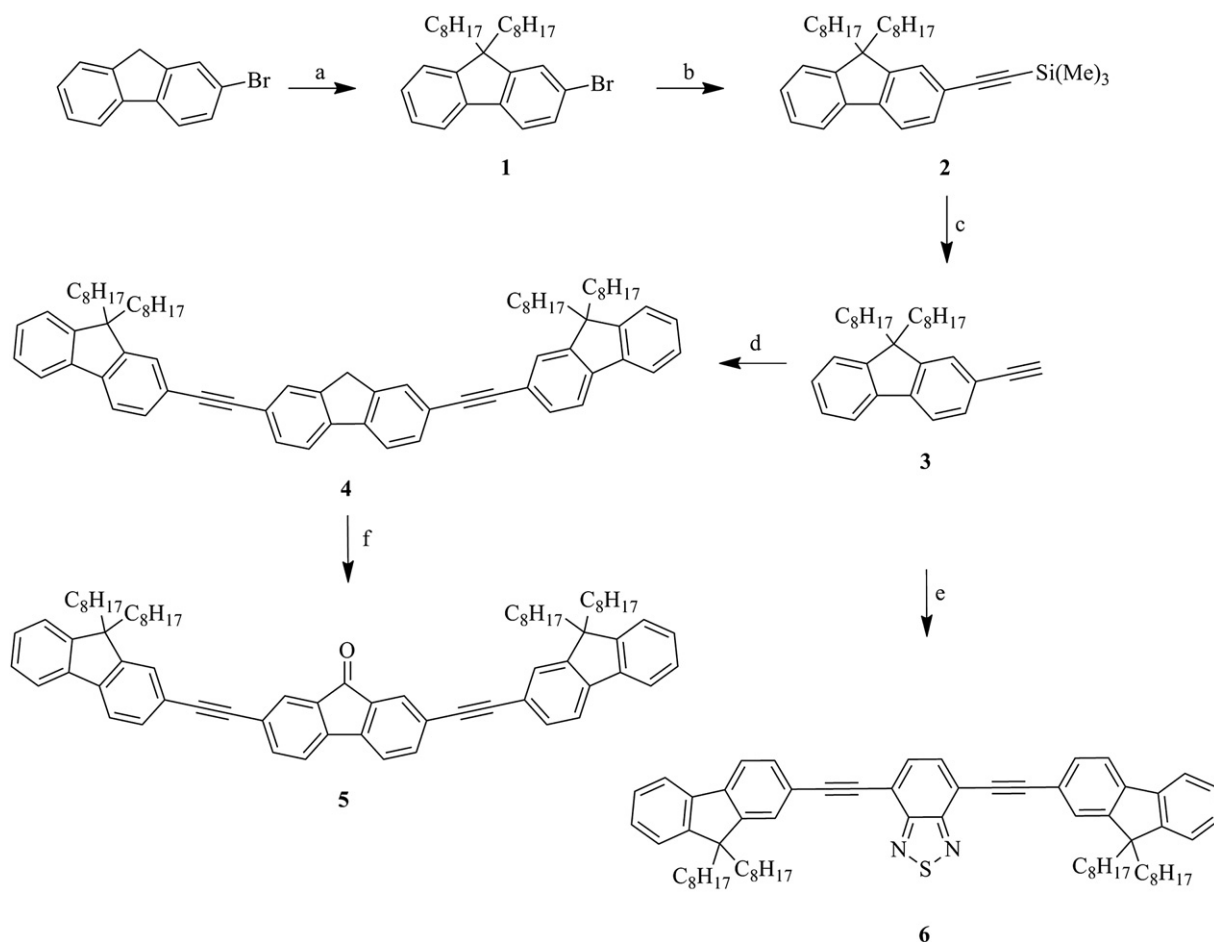
E-mail addresses: [mrodri@cio.mx](mailto:mrodri@cio.mx) (M. Rodríguez), [rsantill@cinvestav.mx](mailto:rsantill@cinvestav.mx) (R. Santillan).

theoretical and experimental results show that the solvent effect on  $\delta_{\text{TPA}}$  values for D- $\pi$ -D and D-A-D systems displayed a non-monotonic behavior with respect to solvent polarity [12,13]. In general, for these  $\pi$ -systems the highest  $\delta_{\text{TPA}}$  values are obtained using solvents with low or intermediate polarity, although sometimes the highest  $\delta_{\text{TPA}}$  values are observed in polar solvents, as in the case of dibenzothiophene core-branched structures [14].

Electronic  $\pi$ -systems containing fluorene rings represent an attractive class of aromatic compounds to build different molecular structures, including those with a D-A-D arrangement [2]. Fluorene has been largely used as donor in D-A materials due to its interesting properties which are a consequence of a large HOMO-LUMO energy gap [15,16]. Moreover, fluorene based systems possess unique photophysical properties such as high fluorescent quantum yield, large optical nonlinearities, large photostability, and excellent hole-transporting properties [17–20]. Due to these properties fluorene derivatives have been used extensively as functional materials for organic light-emitting diodes [21], photodynamic therapy photosensitizers [22], solar cells [23] and fluorescence microscopy [24]. On the other hand, with the oxidation of a fluorene ring it is possible to obtain fluorenone derivatives, which act as acceptor groups favoring the ICT process [25]. This moiety has been also employed for tuning the electronic properties of D-A chromophores [26] and for photovoltaic applications [27–29]. Another moiety of our current interest to tune the photophysical properties in D-A-D systems is the 2,1,3- benzothiadiazole ring. This ring has been widely utilized as acceptor group in combination

with fluorene for the preparation of highly fluorescent green fluorophores [30] and two-photon absorption dyes [31].

In this work, we report the synthesis of novel fluorescent molecules with D-A-D architecture based on fluorenes moieties linked to the acceptors 9-fluorenone and benzothiadiazole rings, for compounds **5** and **6** respectively (see Scheme 1). In the design of **5** and **6** we chose the fluorene ring as donor group since it exhibits excellent photon harvesting and good charge transfer properties toward the acceptor core. We utilized **4** to be a reference material without an acceptor group and in consequence, with no possible ICT character. The aim of our work is to study the effect that has the solvent-solute interaction on the ICT character of our compounds and consequently on their luminescent and non-linear optical properties. The ICT transition for compounds **4–6** was evaluated by solvatochromic studies through steady-state absorption and fluorescence spectroscopy. Then, the strength of the third-order optical nonlinearities that resulted for the ICT character of each compound was first screened by third-harmonic generation experiments and subsequently evaluated in a more detailed way by two-photon absorption studies. Our results demonstrate that the ICT character of these compounds, and the fluorescence induced by TPA, is strongly affected by the utilized solvent, without a monotonic trend with respect to solvent polarity. Such two-photon activity tends to be significantly quenched with solvents of high polarity and with the capacity of producing hydrogen-bonding –such as water– limiting some of the biomedical applications for these compounds, i.e., as labels in fluorescence microscopy. To overcome this



**Scheme 1.** a) 1-Bromooctane, KOH, DMSO; b)  $\text{Me}_3\text{SiC}\equiv\text{CH}$ ,  $\text{Pd}(\text{CH}_3\text{CO}_2)_2$ , CuI,  $\text{PPh}_3$ , DIPA; c)  $\text{K}_2\text{CO}_3$ ,  $\text{MeOH}/\text{Et}_2\text{O}$ ; d) 2,7-Dibromofluorene,  $\text{PdCl}_2(\text{PPh}_3)_2$ ,  $t\text{-BuNH}_2/\text{H}_2\text{O}$ ; e) 4,7-Dibromobenzoc[1,2,5]-thiadiazole,  $\text{PdCl}_2(\text{PPh}_3)_2$ ,  $t\text{-BuNH}_2/\text{H}_2\text{O}$ ; f)  $\text{Cs}_2\text{CO}_3$ , DMSO.

limitation, we prepared an aqueous suspension of nanoparticles synthesized from **6** through the re-precipitation method. We demonstrate that our nanoparticles suspended in water exhibit good two-photon activity (without quenching effects) similar to the activity of solutions prepared with a solvent of intermediate polarity.

## 2. Materials and experimental section

### 2.1. Materials

All starting materials were purchased from Sigma–Aldrich and utilized without further purification. The solvents were purified by distillation over appropriate drying agents.

### 2.2. Equipment

$^1\text{H}$ ,  $^{13}\text{C}$  and two-dimensional NMR spectra were recorded on a Jeol ECA +500 MHz Spectrometer, using deuterated solvents. Electronic absorption spectra were obtained with a Perkin Elmer LAMBDA 2S UV–Vis spectrophotometer. The solution emission spectra were measured on a Varian Cary Eclipse fluorescence spectrometer. Infrared spectra were recorded on an FT–IR Varian ATR spectrometer. High resolution mass spectra were obtained with an Agilent G1969A spectrometer.

### 2.3. Synthesis of compounds 1–6

Compounds (**1–3**) were synthesized according to reported methodologies [32–34].

#### 2.3.1. 2,7-bis((9,9-dioctyl-2-fluorenyl)ethynyl) fluorene (**4**)

Compound **3** (0.26 g, 0.63 mmol), 2,7-dibromo fluorene (0.10 g, 0.31 mmol) and  $\text{PdCl}_2(\text{PPh}_3)_2$  (17 mg, 0.02 mmol) were dissolved in a 1:1 mixture of  $^t\text{-BuNH}_2/\text{H}_2\text{O}$  (6 mL) and the mixture was stirred at room temperature for 48 h. The completion of the reaction was verified by TLC. The organic phase was extracted with ethyl acetate (20 mL) and was washed with water ( $3 \times 20$  mL). The resulting organic solution was dried over anhydrous  $\text{Na}_2\text{SO}_4$  and the solvent was eliminated under vacuum. The crude product was purified by silica gel column chromatography eluting with hexane. Compound **4** was obtained as a colorless oil which solidified adding methanol thereby obtaining a white solid in 15% yield (0.07 g). M.p. = 109–110 °C.  $^1\text{H}$  NMR (500 MHz,  $\text{CDCl}_3$ ):  $\delta$  7.78–7.77 (m, 2H), 7.71–7.68 (m, 2H), 7.61 (dd,  $^3J = 7.7$  Hz;  $^4J = 1.5$  Hz, 1H), 7.55–7.53 (m, 2H), 7.36–7.31 (m, 3H), 3.95 (s, 1H), 1.98 (t,  $J = 8.3$  Hz, 4H), 1.23–1.05 (m, 20H), 0.82 (t,  $J = 7$  Hz, 6H), 0.69–0.59 (m, 4H) ppm.  $^{13}\text{C}$  NMR (125 MHz,  $\text{CDCl}_3$ ):  $\delta$  151.1, 150.8, 143.6, 141.5, 141.2, 140.5, 130.7, 130.6, 128.2, 127.5, 126.9, 126.0, 122.9, 122.0, 121.5, 120.2, 120.0, 119.7, 91.0, 90.1, 55.2, 40.4, 36.6, 31.8, 30.1, 29.3, 23.8, 22.6, 14.1 ppm. IR ( $\nu_{\text{max}}/\text{cm}^{-1}$ ) 2923, 2852 (C–H stretching), 1465 (phenyl). APCI–MS calculated for  $\text{C}_{75}\text{H}_{91} [\text{M} + \text{H}]^+$  991.7115, found 991.7111 [ $\text{M} + \text{H}]^+$  (ppm error of –0.4336).

#### 2.3.2. 2,7-bis((9,9-dioctyl-2-fluorenyl)ethynyl)-9-fluorenone (**5**)

Compound **4** (47 mg, 0.05 mmol) and  $\text{Cs}_2\text{CO}_3$  (46 mg, 0.14 mmol) were dissolved in DMSO (3 mL) and kept at 80 °C overnight. The completion of the reaction was verified by TLC. The organic phase was extracted with ethyl acetate (10 mL) and was washed with water ( $3 \times 10$  mL). The resulting organic solution was dried over anhydrous  $\text{Na}_2\text{SO}_4$  and the solvent was eliminated under vacuum. An orange solid was obtained in 60% yield (28 mg) by preparative silica TLC using hexane:ethyl acetate (96:4) as eluent. M.p. = 98–99 °C.  $^1\text{H}$  NMR (500 MHz,  $\text{CDCl}_3$ ):  $\delta$  7.86(d,  $^4J = 1.0$  Hz, 1H), 7.71–7.68 (m, 3H), 7.54–7.52 (m, 3H), 7.36–7.30 (m, 3H), 1.97

(t,  $J = 8.2$  Hz, 4H), 1.25–1.04 (m, 20H), 0.81 (t,  $J = 7.2$  Hz, 6H), 0.64–0.56 (m, 4H) ppm.  $^{13}\text{C}$  NMR (125 MHz,  $\text{CDCl}_3$ ):  $\delta$  192.4, 151.1, 150.9, 143.2, 141.9, 140.3, 137.7, 134.6, 130.8, 127.7, 127.4, 126.9, 126.1, 124.8, 123.0, 120.9, 120.6, 120.1, 119.8, 92.8, 88.7, 55.2, 40.4, 31.8, 30.1, 29.8, 29.3, 23.8, 22.6, 14.1 ppm. IR ( $\nu_{\text{max}}/\text{cm}^{-1}$ ) 2923, 2848 (C–H stretching), 1716 (C=O), 1465 (phenyl nucleus). APCI–MS calculated for  $\text{C}_{75}\text{H}_{89}\text{O} [\text{M} + \text{H}]^+$  1005.6907, found 1005.6907 [ $\text{M} + \text{H}]^+$  (ppm error of –0.0940).

#### 2.3.3. 4,7-bis((9,9-dioctyl-2-fluorenyl)ethynyl)-2,1,3-benzothiadiazole (**6**)

Compound **3** (0.15 g, 0.37 mmol), 4,7-dibromobenzo[c]-1,2,5-thiadiazole (0.05 g, 0.17 mmol) and  $\text{PdCl}_2(\text{PPh}_3)_2$  (9 mg, 0.01 mmol) were dissolved in a 1:1 mixture of  $^t\text{-BuNH}_2/\text{H}_2\text{O}$  (6 mL) and the mixture was stirred at room temperature for 48 h. The completion of the reaction was verified by TLC. The organic phase was extracted with ethyl acetate (20 mL) and was washed with water ( $3 \times 20$  mL). The resulting organic solution was dried over anhydrous  $\text{Na}_2\text{SO}_4$  and the solvent was eliminated under vacuum. An orange solid was obtained in 50% yield (82 mg) by preparative silica TLC using hexane:ethyl acetate (96:4) as eluent. M.p. = 67–68 °C.  $^1\text{H}$  NMR (500 MHz,  $\text{C}_6\text{D}_6$ ):  $\delta$  7.88 (d,  $^4J = 1.0$  Hz, 1H), 7.70 (dd,  $^3J = 7.7$  Hz,  $^4J = 1.0$  Hz, 1H), 7.49–7.47 (m, 1H), 7.41 (d,  $^3J = 7.7$  Hz, 1H), 7.30 (s, 1H), 7.18–7.13 (m, 3H), 1.90 (m, 4H), 1.15–1.09 (m, 4H), 1.07–0.97 (m, 12H), 0.93–0.87 (m, 4H), 0.77 (t,  $J = 7.2$  Hz, 6H), 0.79–0.71 (m, 4H) ppm.  $^{13}\text{C}$  NMR (125 MHz,  $\text{C}_6\text{D}_6$ ):  $\delta$  154.7, 151.2, 151.1, 142.4, 140.5, 131.9, 131.3, 127.8, 127.1, 126.3, 122.8, 121.6, 120.3, 120.1, 117.5, 98.8, 86.7, 55.2, 40.4, 31.8, 30.1, 29.4, 29.3, 23.9, 22.7, 14.0 ppm. IR ( $\nu_{\text{max}}/\text{cm}^{-1}$ ) 2921, 2852 (C–H stretching), 2200 (C–C triple bond), 1736 (C=N), 1464 (phenyl). ESI-MS calculated for  $\text{C}_{68}\text{H}_{85}\text{N}_2\text{S} [\text{M} + \text{H}]^+$  961.6427, found 961.6428 [ $\text{M} + \text{H}]^+$  (ppm error of 0.0003).

#### 2.3.4. Fabrication of aqueous suspensions of organic nanoparticles

Nanoparticles from our compounds were prepared by using the re-precipitation method: small volumes (200–500  $\mu\text{L}$ ) of THF solution ( $5 \times 10^{-4}$  M) were injected into aqueous solution of Cetyltrimethylammonium bromide (CTAB) (10 mL) at concentration of  $8 \times 10^{-4}$  M under ultrasonic stirring. Molecules began to aggregate at once, and a colloidal suspension of nanoparticles in water was obtained. Excess of THF was eliminated by evaporation under vacuum. The surfactant CTAB was needed to avoid coalescence of nanoparticles. Special care was taken to eliminate large particles by filtering the suspensions with a membrane filter with 0.2  $\mu\text{m}$  cutoff. The resultant samples exhibited high colloidal stability.

#### 2.3.5. Determination of quantum yield

The fluorescence quantum yield ( $\phi$ ) for samples was measured using the integrating sphere method [35], through one-photon excitation provided by a diode-laser (375 nm). The fluorescence quantum yields of samples in solutions were calculated using as reference Rhodamine 6G ( $\phi_{\text{ref}} = 0.95$ ) dissolved in methanol.

#### 2.3.6. Determination of two-photon cross-sections

Two-photon excitation spectra of molecules dissolved in different solvents ( $1 \times 10^{-5}$  M) were measured using the two-photon excited fluorescence technique (TPEF) [36] employing a mode locked Ti:Sapphire laser (Tsunami Spectra-Physics) as excitation source. The laser provided pulses of 100 fs with a pulse repetition frequency of 80 MHz and was tunable in the wavelength range of 750–820 nm. The laser radiation was focused onto a quartz cell of 1 cm of path length (containing the organic solutions or aqueous suspensions of nanoparticles) using a focal lens (5 cm). To avoid linear absorption effects, the beam was focused close to the cell wall. Then the fluorescence emission from solutions of compounds

was focused and recorded on a spectrometer (Ocean Optics USB4000). The measurements were performed in a low excitation intensity regime where the fluorescence signal showed a quadratic dependence on the intensity of the excitation beam. A methanol solution of Rhodamine 6G whose cross-sections values have been completely characterized in the literature [37], was employed as a reference for calculations. The TPA cross-sections were calculated at each wavelength according to Eq. (1), where  $C(C_{\text{ref}})$  and  $n(n_{\text{ref}})$  are the concentration and refraction index of the sample(reference), respectively, and  $F(F_{\text{ref}})$  is the integral of the TPEF spectrum.

$$\delta_{\text{TPA}} = \delta_{\text{ref}} \frac{\phi_{\text{ref}} C_{\text{ref}} n_{\text{ref}} F}{\phi C n F_{\text{ref}}} \quad (1)$$

### 2.3.7. Third-harmonic generation (THG) experiments

Non-linear optical properties of our compounds in solid films were evaluated by the well-known THG Maker fringe technique. Polystyrene thin films doped with these chromophores (30 %wt) were deposited over glass substrates using the spin-coating method. Briefly, the THG experiments consist on focusing infrared laser pulsed irradiation (nanosecond pulses at a repetition rate of 10 Hz) into the films. Then the intensity of the third-harmonic beam that emerges from the films is measured and the third-order non-linear susceptibility is calculated according to THG Maker fringes approach [38]. For details of our THG Maker fringe setup see previous work [39].

## 3. Results and discussion

### 3.1. Synthetic strategy

The alkylation reaction of 2-bromofluorene with 1-bromooctane using KOH as base in DMSO gave **1** in excellent yield (Scheme 1). Subsequent treatment of compound **1** with ethynyltrimethylsilane under Sonogashira cross-coupling conditions produced compound **2**. The hydrolysis reaction of **2** to obtain **3** was carried out with  $\text{K}_2\text{CO}_3$  in a MeOH/Et<sub>2</sub>O solvent mixture.

Sonogashira cross-coupling reaction of **3** and 2,7-dibromofluorene or 4,7-dibromobenzo[c]-1,2,5-thiadiazole using  $\text{PdCl}_2(\text{PPh}_3)_2$  as catalyst, in the absence of copper (to prevent Glaser-type oxidative homocoupling) with solvent mixtures of *t*-BuNH<sub>2</sub>/water [40] afforded **4** and **6**. Compound **5** was obtained in 60% yield by oxidation of the central methylene group in **4** with  $\text{Cs}_2\text{CO}_3$  in DMSO [41]. The structures of compounds **4**, **5**, and **6** were established using <sup>1</sup>H and <sup>13</sup>C NMR spectra and two-dimensional (COSY, HETCOR and HMBC) experiments. The <sup>13</sup>C NMR spectra of compounds **4** to **6** show characteristic signals. The <sup>13</sup>C NMR spectra of compound **4** (see Fig. S1 of supporting information) shows a signal at 36.6 ppm that corresponds to the CH<sub>2</sub> moiety, whereas for compound **5** the signal at 192.4 ppm confirms the oxidation of the methylene moiety to the corresponding keto group (Fig. S2). The chemical shift for the acetylene fragment signals in **6** (98.8 and 86.7 ppm) shows a large difference with respect to the same signals in derivatives **4** (91.0 and 90.1 ppm) and **5** (92.8 and 88.7 ppm), probably due to the more electronegative nature of the benzo-thiadiazole ring compared to the fluorene/fluorenone core. The signal at 154.7 ppm was assigned to the C=N fragment of benzo-thiadiazole (Fig. S3). The derivatives **4–6** were obtained as stable solids and they were soluble in common organic solvents. Since previous reports have provided evidence that some ethynylbenzothiadiazole derivatives are unstable at room conditions

[42], the photostability of compounds **6** in solution and colloidal suspension was evaluated (*vide infra*).

### 3.2. IR spectroscopy

The infrared spectra of **4**, **5** and **6** show characteristic bands for each compound that corroborate the formation of ethynylfluorene derivatives. For compound **4** only the aliphatic groups near 3000 cm<sup>-1</sup> and the aromatic moiety at 1465 cm<sup>-1</sup> are observed. For compound **5** the characteristic band for the carbonyl group appears at 1716 cm<sup>-1</sup>. Finally, the spectrum of compound **6** shows the band at 1736 cm<sup>-1</sup> that is attributed to C=N stretching and the alkyne stretching observed at 2200 cm<sup>-1</sup> (Fig. S4).

### 3.3. Linear absorption and fluorescence spectra

Absorption spectra of compounds **4–6** were obtained in different solvents such as hexane, toluene, dioxane, tetrahydrofuran, acetone, acetonitrile and methanol to evaluate the influence of the polarity of the medium over their photophysical properties. In particular, we were interested in studying the ICT transition in **5** and **6** (each compound with different donor–acceptor capabilities).

The linear absorption spectra of compounds **4**, **5** and **6** are shown in Fig. 1 and the main characteristics are summarized in Table 1 (compounds **4** and **5** are insoluble in polar solvents due to their hydrophobic character). In the absorption spectrum of **4** there is one intense band in the range 369–374 nm. This band is assigned to a  $\pi \rightarrow \pi^*$  electronic transition and its shape is very similar to the one produced by fluorene [43]. For compound **5**, although four bands are distinguished, our interest was focused on those at 366–370 nm ( $\pi \rightarrow \pi^*$ ) and 439–449 nm, respectively. In the case of compound **6**, a “camel back” spectrum shape is observed with two strong absorption bands around 319–321 ( $\pi \rightarrow \pi^*$ ) and 431–441 nm. According to previous reports [44,45], the intense bands observed in the range 431–449 nm in **5** and **6** should correspond to an ICT transition that occurs between the fluorene edge units and the fluorenone and benzothiadiazole central cores, respectively. This affirmation is supported by the absence of an absorption band at visible wavelengths – assigned in **5** and **6** as ICT transition bands – in the spectrum of compound **4** due to the absence of an acceptor group, so that ICT is improbable in such compound. Then, the inclusion of stronger acceptor groups in **5** and **6** within the electronic  $\pi$ -system induces a decrease in the intensity of the  $\pi \rightarrow \pi^*$  transition (see molar absorption coefficients for compounds **5** and **6** compared with **4** in Table 1) and also leads to the appearance of the ICT band [46]. Table 1 also shows that the position of the  $\pi \rightarrow \pi^*$  electronic transitions in different solvents are practically independent of solvent polarity. As for the ICT bands, it is known that they usually show bathochromic shifts when the solvent polarity is increased, however, in the case of derivatives **5** and **6** only slight shifts were recorded with a non-monotonic behavior. In any case, it is known that the absorption spectra are less sensitive to polarity changes in comparison with the emission spectra [2,47].

The photoluminescence (PL) spectra for **4**, **5** and **6** derivatives were also obtained in different solvents using 360, 310 and 320 nm as excitation wavelengths, respectively (see Fig. 2). The corresponding wavelengths of maximum emission, intensity of emission and Stokes shifts are summarized in Table 2, as well as the quantum yield values for **6**. The well-defined vibronic PL spectrum (blue light emission) of **4** is typically observed in fluorene derivatives [49]; this PL spectrum from **4** did not change significantly in different solvents. In contrast, no significant PL generated by fluorene moieties was observed from **5** and **6**. The quenching of the emission of the fluorene moiety is compatible either with a charge transfer process from the fluorenes to the acceptor core center [44,50], or with an

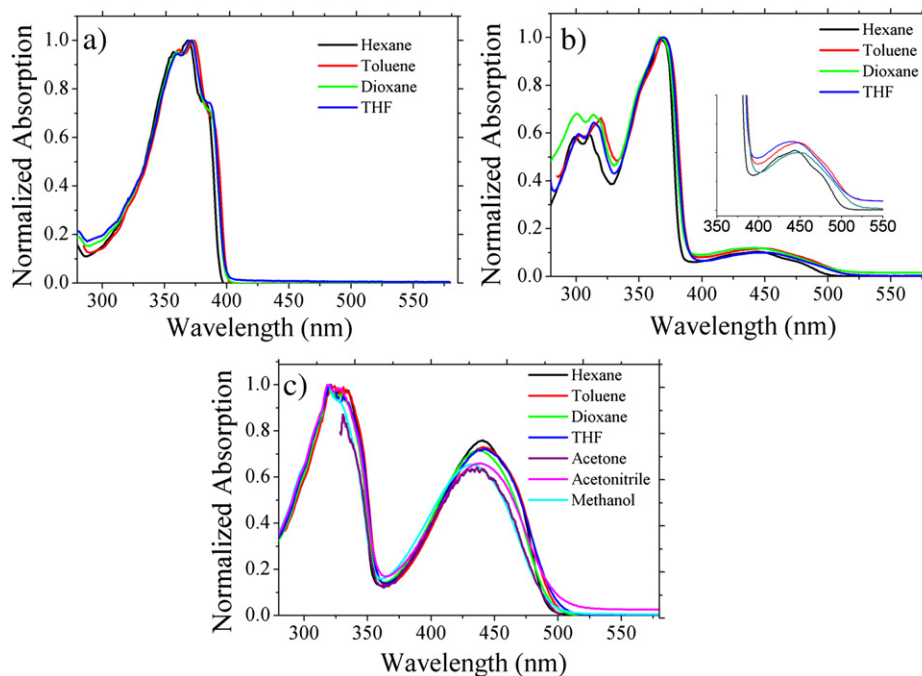


**Fig. 1.** UV–Vis normalized absorption spectra of a) **4**, b) **5** and c) **6** in different solvents (molar absorption spectra for **6** are shown in Fig. S5). Inset in b) shows an enlargement of the region where the ICT band appears.

energy transfer process, although the latter is rather related to bimolecular systems [51]. For derivative **5** a very weak blue emission was detected (inset of Fig. 2b), this behavior was associated with an incomplete ICT process. Indeed, as shown in Figs. 1 and 2, there is an overlap between the emission spectrum of **4** (band generated by the fluorene moiety) and the ICT band in the absorption spectra of **5** and **6**. Thus, it can be concluded that the acceptor moieties in **5** and **6** are responsible for the luminescent processes. For these two compounds, slightly structured emission bands are observed in hexane solution at 507 and 495 nm, respectively, but when moderate polar solvents are used, a broad and unstructured band is recorded. It is noteworthy that the PL spectra from compound **6** are strongly dependent on the solvent polarity, going from greenish emission in hexane solution to reddish in methanol (see Table 2 and Fig. 2c and d).

Compound **6** exhibited the most intense PL and significant ICT character, so that we selected it for additional spectroscopic studies. Firstly, to verify the ICT character of this molecule we obtained its excitation spectrum. Fig. 3a presents the PL intensity detected at 511 nm for **6** dissolved in toluene. As expected, the largest green

emission was recorded with the excitation from 320 to 340 nm, corroborating that the PL properties of compound **6** are due to the ICT. In general, the wavelength of maximum emission for this derivative shows a monotonic shift effect when the solvent polarity is increased. This bathochromic shift was accompanied with changes in the fluorescence quantum yield (see Table 2). Results show a significant reduction for this photophysical property going from non-polar aprotic to polar protic solvents. Acetone, acetonitrile and THF solutions gave quantum yields higher than 0.85, however, in methanol, there was a drastic PL quenching ( $\phi = 0.3$ ) which was assigned to hydrogen-bonding interactions between the solvent and benzothiadiazole core [47,52,53]. The quenching was also observable in mixtures of solvents. For instance, Fig. 3b displays the PL spectra of compound **6** (at concentration of  $6 \times 10^{-5}$  M) in mixtures of THF-methanol. The data shows that as the ratio of methanol present in the solution is increased, the emission band undergoes a bathochromic shift. A reduction of the PL intensity is also clearly observed. From this, one can infer that in a protic polar solvent like water, the fluorescent properties of compound **6** would be also quenched, precluding then its application in areas for which aqueous solutions of these type of molecular systems are of major

**Table 1**

One-photon absorption data for compounds **4–6** obtained in different solvents.

Solvent	P. I. <sup>a</sup>	Compound 4	Compound 5	Compound 6		
		$\lambda\pi \rightarrow \pi^*$ <sup>b</sup> (ε) <sup>c</sup>	$\lambda\pi \rightarrow \pi^*$ <sup>b</sup> (ε) <sup>c</sup>	$\lambda_{\text{ICT}}$ <sup>b</sup> (ε) <sup>c</sup>	$\lambda_{\text{ICT}}$ <sup>b</sup> (ε) <sup>c</sup>	
Hexane	0.009	369(85,100)	366(7900)	444(820)	320(43,450)	441(33,000)
Toluene	0.099	374(84,000)	370(8780)	449(1040)	320(47,600)	441(34,750)
Dioxane	0.164	372(96,000)	368(7040)	439(840)	320(43,550)	438(31,200)
THF	0.207	372(57,500)	369(8350)	445(830)	321(51,950)	441(37,500)
Acetone	0.355				320(87,200)	435(63,400)
Acetonitrile	0.460				319(36,560)	431(23,900)
Methanol	0.762				320(25,300)	439(16,700)

<sup>a</sup> Polarity Index see ref [48].

<sup>b</sup> Value expressed in nanometers.

<sup>c</sup> Value expressed in  $\text{M}^{-1} \text{cm}^{-1}$ .

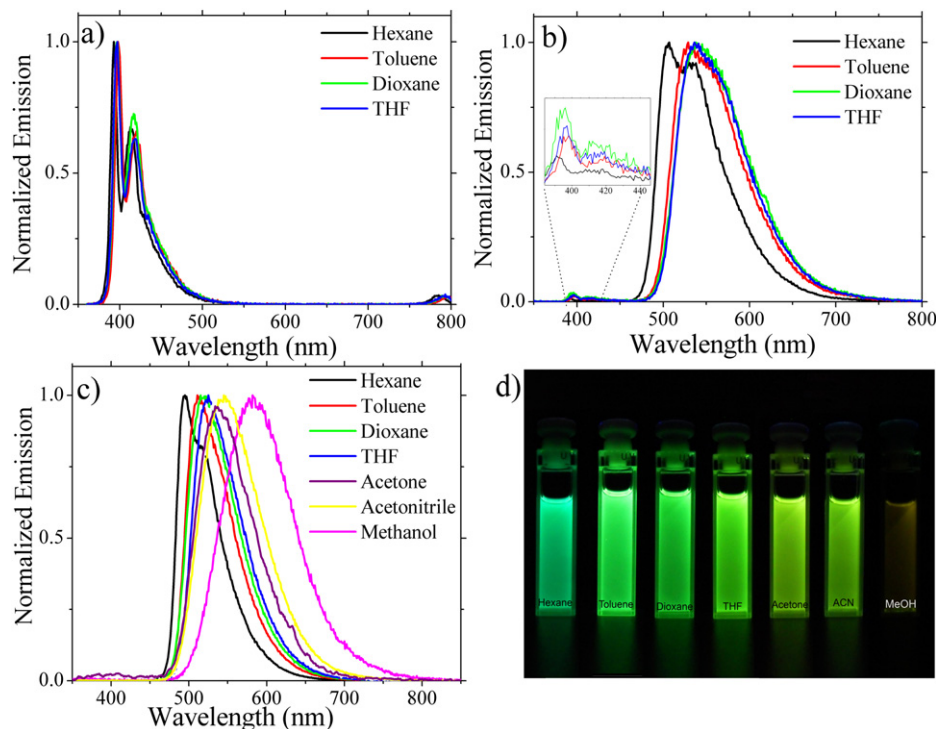


**Fig. 2.** Emission spectra of a) **4**, b) **5** and c) **6** in different solvents; d) photograph of solvatochromism effect for compound **6** under UV lamp excitation: from left to right hexane, toluene, dioxane, THF, acetone, acetonitrile (ACN) and methanol solutions.

interest, i.e., for fluorescent microscopy. Nevertheless, we demonstrate in Section 3.6 that in mixtures of THF-water the quantum yield of **6** can be conserved after molecular aggregation.

### 3.4. General solvent effects evaluated by Lippert–Mataga relation

In order to explain the effect of the polarity of the medium, and to determine whether general and/or specific solvent effects [47] are responsible for the spectral shifts in the emission of compound **6**, we applied the Lippert–Mataga relation. For general type effects, the fluorophore is considered as a dipole in a continuous medium of uniform dielectric constant. The general effects are determined by the electronic polarizability of the solvent; those effects are described by the refractive index and the molecular polarizability, which results from reorientation of solvent dipoles. Molecular polarizability is a function of the static dielectric constant,  $\epsilon$ . In contrast, specific solvent effects are interactions

determined by chemical properties of the fluorophore and the solvent, including hydrogen-bonding, preferential solvation and molecular charge transfer interactions [53]. The Lippert–Mataga plot shows the relation between Stokes shift and the solvent polarity according to [54]:

$$\Delta\bar{\nu} = \bar{\nu}_A - \bar{\nu}_F = \frac{2}{hc} (\Delta f) \frac{(\mu_e - \mu_g)^2}{a^3} + C \quad (2)$$

where  $\bar{\nu}_A$  and  $\bar{\nu}_F$  are the wavenumbers (in  $\text{cm}^{-1}$ ) of the absorption and emission bands, respectively,  $h = 6.6256 \times 10^{-27}$  J s is Planck's constant,  $c = 2.9979 \times 10^{10}$  cm/s is the speed of light,  $a$  is the Onsager radius [55], and  $\Delta\mu = \mu_e - \mu_g$  is the dipole moment difference between the ground and excited states. The solvent polarity  $\Delta f$  is defined in terms of the dielectric constant ( $\epsilon$ ) and the refractive index ( $n$ ) of solvent as (Eq. (3)):

**Table 2**  
Emission data for derivatives studied in different solvents.

Solvent	Compound 4 <sup>a</sup>		Compound 5 <sup>b</sup>		Compound 6 <sup>c</sup>		
	$\lambda_{em}^d$ (I. E.) <sup>e</sup>	Stokes shift <sup>f</sup>	$\lambda_{em}^d$ (I. E.) <sup>e</sup>	Stokes shift <sup>f</sup>	$\lambda_{em}^d$ (I. E.) <sup>e</sup>	$\phi^g$	Stokes shift <sup>f</sup>
Hexane	393(230)	1655	507(370)	7599	495(670)	0.85	11,048
Toluene	398(180)	1612	529(180)	8123	511(530)	0.76	11,681
Dioxane	397(190)	1693	538(120)	8587	515(530)		11,833
THF	397(170)	1693	536(160)	8443	525(540)	0.87	12,105
Acetone					541(720)	1	12,766
Acetonitrile					545(440)	0.9	12,999
Methanol					582(120)	0.3	14,068

<sup>a</sup> Concentration  $1.0 \times 10^{-5}$  M.  $\lambda_{ex} = 360$  nm. The slit aperture was of 1.5 for excitation and 2.5 for emission.

<sup>b</sup> Concentration  $5.2 \times 10^{-5}$  M.  $\lambda_{ex} = 310$  nm. The slit aperture was of 2.5 for excitation and emission.

<sup>c</sup> Concentration  $5.2 \times 10^{-5}$  M.  $\lambda_{ex} = 320$  nm. The slit aperture was of 2.5 for excitation and emission.

<sup>d</sup> Value expressed in nm.

<sup>e</sup> Intensity emission expressed in arbitrary units.

<sup>f</sup> Value expressed in  $\text{cm}^{-1}$ .

<sup>g</sup> Rhodamine 6G methanol solution ( $\phi = 0.95$ ) was utilized as reference.

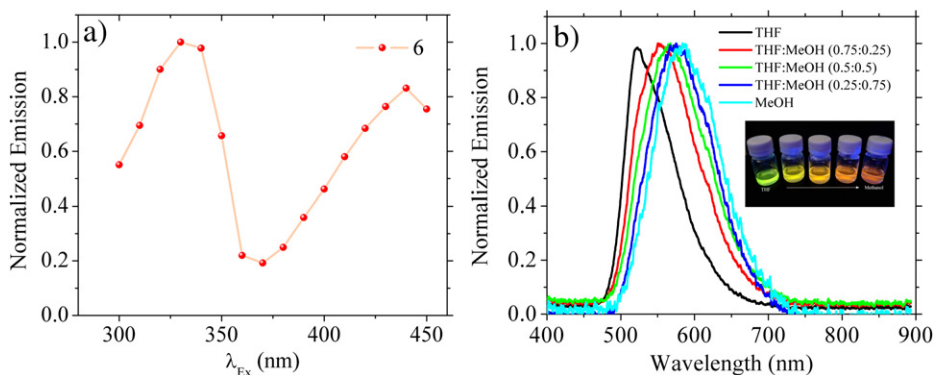


**Fig. 3.** a) Excitation spectrum from **6** in toluene solution. The PL is detected at 511 nm b) PL spectra of compound **6** in mixtures of THF-methanol. The concentration of **6** in these mixtures was kept constant ( $6 \times 10^{-5}$  M). Inset photography of the PL exhibited by the mixtures.

$$\Delta f = f(\epsilon) - f(n^2) = \left( \frac{\epsilon - 1}{2\epsilon + 1} - \frac{n^2 - 1}{2n^2 + 1} \right) \quad (3)$$

It is known that when Lippert–Mataga plots exhibit a linear behavior the general solvent effects are dominant in the spectral shifts. On the other hand, when Lippert plots are non-linear, the specific solvent effects govern the spectral shifts and it is regarded as evidence of specific fluorophore–solvent interactions. Fig. 4 presents the Stokes shift as a function of the solvent polarity for compound **6**. Clearly, data in this plot deviates from linearity (line not shown in the figure with slope =  $6020 \pm 1485$ ,  $R^2 = 0.72$ ), and a bilinear behavior is observed: i) the first linearity for the non-polar region ( $\Delta f < 0.03$ ; slope =  $38,449 \pm 7926$ ,  $R^2 = 0.918$ ) includes hexane, toluene and dioxane, and ii) the second linearity for the polar region ( $\Delta f > 0.2$ ; slope =  $9286 \pm 395$ ,  $R^2 = 0.996$ ) includes only THF, acetone and acetonitrile (ACN). The nonlinearity observed as a general trend going from hexane to acetonitrile can be related to ICT as specific interaction while methanol deviation was assigned to intermolecular hydrogen-bonding [56] in addition to ICT.

From the Lippert–Mataga plots, the  $\Delta\mu$  values can be obtained to allow an estimation of the dipole moment of the emitting excited state. It should be also noted that according to the D–A–D character of **6**, the states involved in absorption transitions have no significant permanent ground-state dipole moment, so that the values of  $\Delta\mu$  are mostly related to polar emitting excited states. Then, from the slope of the polar region [57] on the Lippert–Mataga plot – the region with the best approximation – we estimated the

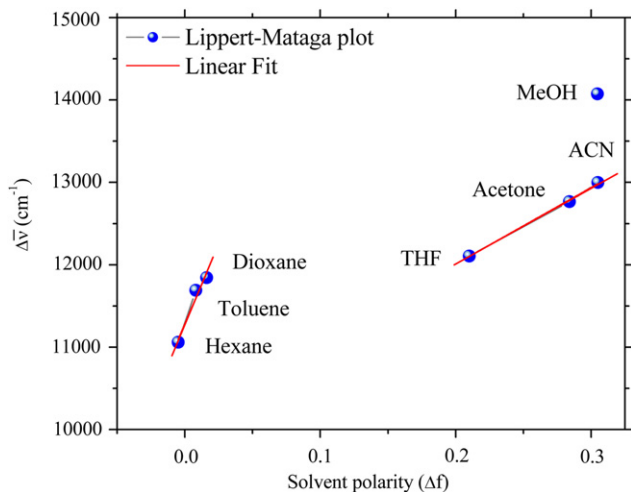


**Fig. 4.** Lippert–Mataga plot of **6** in seven pure solvents.

dipole moment difference between the ground and excited state ( $\Delta\mu$ ) to be 15.3 D, taking an Onsager radius of 6.33 Å estimated by a Density Functional Theory (DFT) calculation using Gaussian 03 [58]. In this procedure the tight option was selected for a better computational accuracy. Onsager radii 0.5 Å longer than the computed radii are chosen to account for the van der Waals radii of the surrounding solute molecules. This  $\Delta\mu$  value is only an approximation, but is comparable with those reported in the literature (3–20 D) for other solvatochromic fluorophores [59].

### 3.5. Theoretical studies

With the purpose of corroborating the origin of the electronic transitions involved in the studied compounds, we calculated Frontier Molecular Orbitals (FMOs) obtained by the Density Functional Theory (DFT) at the B3LYP/6-31G\* level of theory using the Gaussian 03 code [58]. The optimized ground-state geometry and the corresponding FMOs are shown in Fig. 5. It can be seen that the three modeled molecules exhibit practically a planar geometry. We assumed three possible conformations: a) with the methylene bridge of the terminal fluorenes in different directions (one of them parallel to the core); b) both methylene bridges of the fluorenes parallel to the core and c) both methylene bridges of the fluorenes opposite to the core, ensuring by frequency analysis that all these conformers are local minima, for which no imaginary points were found. Fig. 5 shows the FMOs of the three derivatives in the more stable conformation and Table 3 summarizes the most important results for electronic excitations and oscillator strength values. For compound **4**, we found that HOMO → LUMO was the transition ( $\pi \rightarrow \pi^*$ ) with the highest contribution. For compound **5**, analysis showed the existence of three principal transitions: HOMO → LUMO + 2, HOMO → LUMO + 1 and HOMO → LUMO at 353, 358 and 432 nm, respectively; while for derivative **6**, the principal transitions are: HOMO → LUMO + 1 and HOMO → LUMO located at 361 and 551 nm respectively. These results clearly demonstrate that for both **5** and **6** the transitions at low energies are associated to HOMO levels with a  $\pi$  type bonding character and electronic density delocalized on the complete molecular frame; whereas for the LUMO levels, the electronic density was redistributed and confined to the central acceptor moieties. Therefore the HOMO → LUMO transitions involve an ICT process. At higher energies such ICT process is no longer observed and it is replaced by  $\pi \rightarrow \pi^*$  transitions.

The oscillator strength values for compounds **4**, **5** and **6** were also estimated in the framework of ZINDO without taking into account solvent effects (see Table 3). The computed values on the semiempirical optimized geometry for the HOMO → LUMO

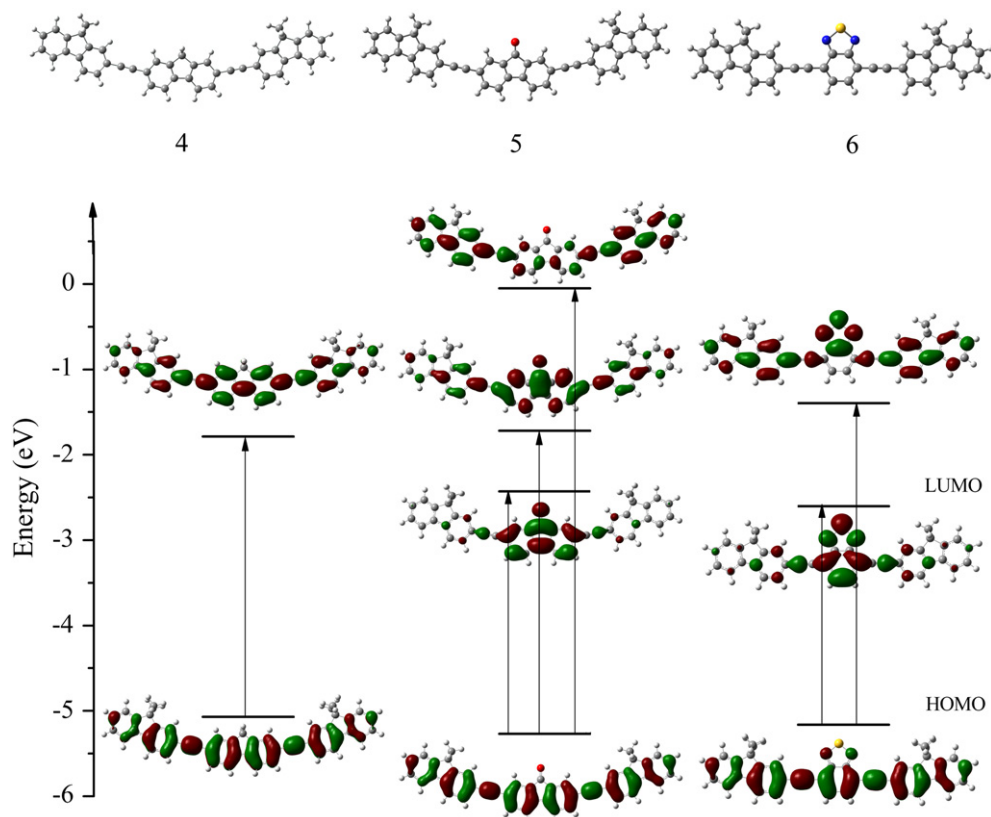


Fig. 5. Gas-phase orbital pictures for **4**, **5** and **6** in the frontier region. For compounds **5** and **6** it is evident that the lower transitions, i.e., HOMO  $\rightarrow$  LUMO undergo a redistribution of electronic density from the entire frame to only the acceptor core center.

electronic transition for **4** and HOMO  $\rightarrow$  LUMO and HOMO  $\rightarrow$  LUMO + 1 for **5** and **6** resulted overestimated, observing a red-shift compared to the experimental absorption bands. These red-shifted values can be related to a complete delocalization in the system, which is a consequence of a totally planar arrangement. However, these bathochromic shifts are observed for the three molecules showing the same trend in the oscillator strength estimation.

### 3.6. Photophysical properties from aqueous solutions of nanoparticles

The alkyl chains present in derivatives **4–6** provide a hydrophobic character that favors the self agglomeration and formation of nanoparticles (nanoagglomerates) in water. Aqueous suspension

**Table 3**  
Oscillator strength of simulated electronic spectra and major transition contributions for compounds **4–6**.

Compound	Experimental absorption <sup>a</sup>	Theoretical absorption <sup>a</sup>	Oscillator strength	Transition	Contribution (%)
<b>4</b>	369	391	2.4654	H - 1 $\rightarrow$ L+1	8
				H $\rightarrow$ L	33
<b>5</b>	444	432	0.9111	H $\rightarrow$ L	35
				H - 1 $\rightarrow$ L + 2	9
	366	358	1.525	H $\rightarrow$ L + 1	27
				H - 1 $\rightarrow$ L	11
<b>6</b>	441	551	0.9115	H $\rightarrow$ L	43
				H $\rightarrow$ L + 1	27
	320	361	1.0249	H $\rightarrow$ L + 1	27
				H $\rightarrow$ L + 2	17

<sup>a</sup> Value expressed in nm.

of colloidal nanoparticles of compound **6** (**6NP**) was prepared using a modification of the re-precipitation process reported by Nakanishi and coworkers [60]. The surfactant agent (CTAB) was employed to reduce the surface tension of the nanosystem. Fluorescent nanoparticles with diameter smaller than 200 nm were obtained (see inset in Fig. 6b). The suspension was stable at room temperature for several months.

The absorption and PL spectra from aqueous suspensions of **6NP** are shown in Fig. 6. A comparison of the **6NP** spectrum with those obtained for **6** in solution (Fig. 1) reveals that the  $\pi \rightarrow \pi^*$  transition appears again at 319–320 nm, however, the peak for ICT transition is now slightly red shifted to 447 nm. The PL spectrum of **6NP** shows an unstructured band at 522 nm, a wavelength than lies between that observed for the PL peaks in solutions of dioxane (515 nm) and THF (525 nm). The quantum yield of **6NP** in water was surprisingly high, giving a value of  $\phi = 0.83$ ; such a value is close to the values determined in THF ( $\phi = 0.87$ ) and in hexane ( $\phi = 0.85$ ) solutions (see Table 2). The optical properties were maintained for several months without degradation, since the hydrophobic environment created by the molecules of surfactant that surround the **6NP** provided stabilization. We also prepared aqueous suspensions of **6NP** without the use of surfactant, obtaining nanoparticles that were stable only for a few days, and after that time the formation of a precipitate was observed. Nevertheless, we could observe that the optical properties of the nanoparticles synthesized with and without surfactant were the same.

As far as the fluorophores are concerned, one of the most important properties is their photostability. In order to evaluate the photostability of derivative **6**, we carried out a continuous UV–Vis irradiation on a THF solution under aerobic conditions over 2 h. As irradiation source we used a Xenon lamp (150 W). In addition, the

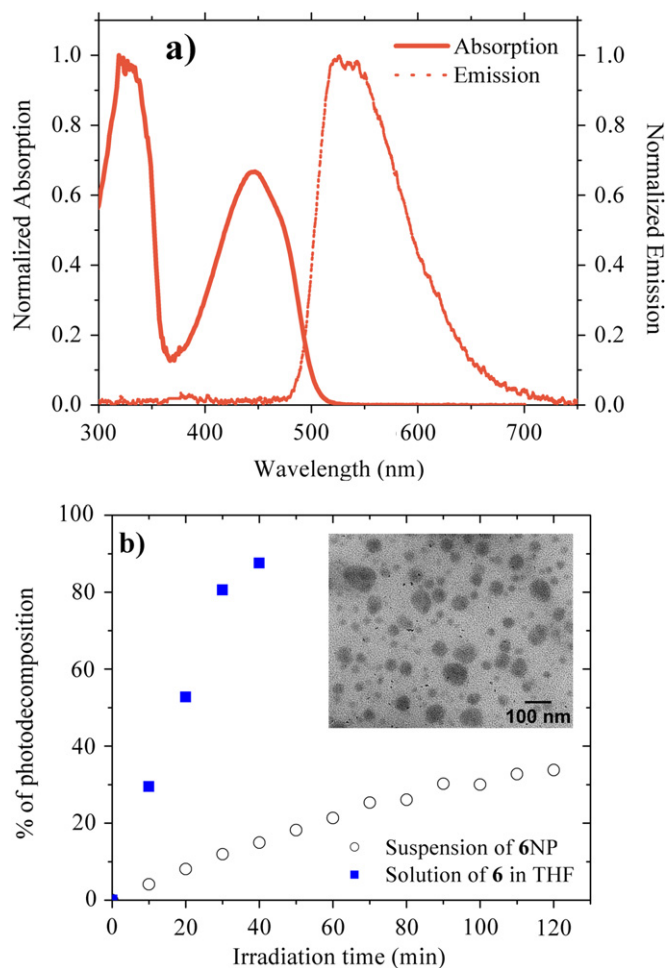


**Fig. 6.** a) Absorption and PL spectra of **6NP**. b) Percentage photodecomposition of compound **6** in THF solution (filled squares) and aqueous nanoagglomerates (open circles). Inset. TEM micrographs of **6NP** obtained from suspension processed using solution of CTAB at 0.8 mM.

photostability of **6NP** in water was also evaluated under the same experimental conditions. The photodegradation of compound **6** in solution and **6NP** was quantified by monitoring the decrease of absorption intensity at 447 nm (see Fig. 6b). The THF solution showed significant photodegradation, with almost 90% of photodecomposition observed after 40 min of irradiation; in contrast, the suspension of **6NP** showed only 33% of degradation after 120 min. Clearly the experimental results indicate that the formation of nanoagglomerates leads to high photostability.

### 3.7. Non-linear optical characterization

Coherent frequency conversion experiments were implemented to obtain a first insight on the non-linear optical properties of our compounds. In particular, we detected the THG produced from solid polystyrene thin films ( $\sim 150$  nm) doped with either **5** or **6**.

The samples were pumped at 1200 nm corresponding to a THG wavelength of 400 nm. For fluorene derivative **5** the THG response was lower than our experimental detection limit, while derivative **6**, having a D–A–D structure with a stronger ICT character, produced an easily detectable THG signal. This clearly demonstrates how the ICT contributes to enhance the nonlinearities. The cubic non-linear susceptibility  $\chi^3(-3\omega; \omega, \omega, \omega)$  from thin films of **6** was  $3 \times 10^{-12}$  esu, calculated by means of THG Maker Fringes formalism. This value is comparable to the value of  $4.3 \times 10^{-12}$  esu reported for fluorene polymers containing similar electronic structure [61].

TPA properties, associated to the cubic non-linear susceptibility tensor of type  $\omega^3(-\omega; \omega, -\omega, \omega)$ , were also evaluated. Taking advantage of the PL exhibited by solutions of our fluorene derivatives, we obtained the TPA cross-sections ( $\delta_{\text{TPA}}$ ) for compounds **5** and **6** using the TPEF technique with femtosecond laser pulses, as described in the experimental section. Table 4 summarizes a comparison between the  $\delta_{\text{TPA}}$  values measured at 750 nm using different solvents (for compound **5**, TPA properties were studied only in four solvents due to insolubility characteristics). From this table we clearly observe how the strong ICT over the electronic D–A–D structure of **6** impacts the nonlinearities: the maximum  $\delta_{\text{TPA}}$  observed in **6** ( $\sim 1000$  GM in THF) is about ten times larger with respect to the maximum value in **5** (105 GM in hexane). Such a TPA effect in **6** is comparable with recent reports on D–A–D structures. For instance, Cheng et al. [62] observed values of  $\delta_{\text{TPA}} \sim 1600$  GM when they used diphenylamine and benzothiadiazole moieties as D and A, respectively, and fluorene units as  $\pi$ -bridges. Similarly, Wang et al. measured  $\delta_{\text{TPA}}$  values up to 2103 GM (with  $\phi \sim 0.36$ ) in THF solutions of a D–A–D compound containing a benzothiadiazole core and fluorene units as a  $\pi$ -bridges [31a]; note that in this case the two-photon activity (the product of  $\phi \times \delta_{\text{TPA}}$ ) is similar to the activity of **6**. The enhanced TPA properties observed in **6** can also be visualized by comparison with other D–A–D systems that employed benzothiadiazole as acceptor group but lack the presence of fluorene units in their structure, i.e., in the representative works performed by Kato et al. in a variety of such compounds they obtained  $\delta_{\text{TPA}}$  in the range 43–330 GM [31b]. Small chromophores with D– $\pi$ -A structure comprising fluorene units also display similar  $\delta_{\text{TPA}}$ , although the TPA effect can be certainly improved incorporating fluorene moieties into multibranching chromophores to reach values of  $\delta_{\text{TPA}}$  in the order of 600–3000 GM [63].

Fig. 7a display the dispersion curves of  $\delta_{\text{TPA}}$  measured for **6** in different solvents and **6NP** in water. The recorded data indicate that for all solvents the maximum TPA cross-sections for **6** is obtained at 750 nm, with a maximum value of nearly 1000 GM in THF solution. However, the non-linear response decreases notably in hexane, acetonitrile and methanol solutions, with measured  $\delta_{\text{TPA}}$  values of 317, 238 and 236 GM, respectively. Meanwhile, the TPA spectrum of **6NP** in water shows a maximum  $\delta_{\text{TPA}}$  value of 514 GM at 750 nm. This value is approximately half of the maximum value recorded in THF solution. To summarize these results, Fig. 7b presents the maximum value of  $\delta_{\text{TPA}}$  for **6** as a function of solvent dielectric constant. We can see that  $\delta_{\text{TPA}}$  has a non-monotonic behavior with respect to the dielectric constant. It is evident that the interaction between the chromophore and solvent molecules produced enhanced ICT process (which is the basis of TPA response) with

**Table 4**  
Summary of  $\delta_{\text{TPA}}$  values of compounds **5** and **6** at 750 nm.

Compound	Hexane	Toluene	THF	Acetone	Acetonitrile	Methanol	Nanoparticles
<b>5</b>	105	81	23	–	–	–	–
<b>6</b>	317	819	1000	660	238	236	514

TPA cross-section given in GM units ( $1 \text{ GM} = 10^{-50} \text{ cm}^4 \text{ s}$ ).

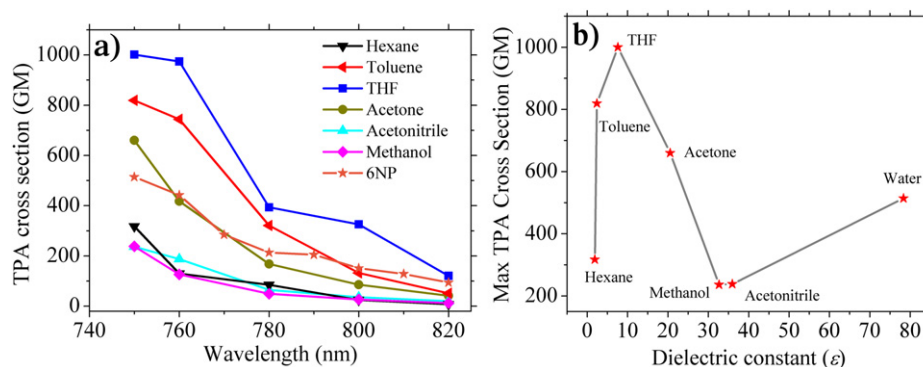


Fig. 7. a) TPA spectra of compound **6** dissolved in hexane, toluene, THF, acetone, methanol, acetonitrile. For comparison, the spectrum corresponding to **6NP** dispersed in water is included. b) Non-monotonic behavior of the maximum  $\delta_{\text{TPA}}$  of **6** as a function of dielectric constant for each solvent.

medium polar solvent such as THF, but such process was considerably reduced in non-polar (hexane) and polar (methanol) solvents. For the case of methanol, chromophore–solvent interactions were also responsible for strong fluorescence quenching effects. In view of the  $\delta_{\text{TPA}}$  values exhibited by **6** in different solvents, it is noteworthy that **6NP** tends to retain good  $\delta_{\text{TPA}}$  values in spite they are immersed in a high polar medium such as water. Furthermore, it can be pointed out that the fluorescence quantum yield measured from **6NP** resulted to be  $\phi = 0.83$ . The relatively large  $\delta_{\text{TPA}}$  values and high quantum yield exhibited by **6NP** are attractive properties; in fact the two-photon activity of our nanoagglomerates is larger than those measured for commercial biomarkers, i.e., Rhodamine-Phalloidin with  $\sim 80$  GM, utilized in fluorescence microscopy [13].

#### 4. Conclusions

Three novel stable fluorene derivatives (**4–6**) were prepared, with **5** and **6** having D–A–D architecture; the linear and non-linear absorption and the photoluminescence properties were recorded in several solvents. These photophysical properties were strongly affected by the solvents and did not show a monotonic trend with respect to solvent polarity. The Lippert–Mataga plot revealed a non-linear behavior due to specific solvent effects, i.e., ICT, for the range of solvents used in this experiment. Theoretical studies showed that for compounds **5** and **6** the low-lying absorption band presents an ICT character because the LUMO is located over the fluorenone and benzothiadiazole group, respectively. The strong ICT character for compound **6**, induced the largest two-photon activity among the studied compounds, with a maximum two-photon absorption cross-section of  $\delta_{\text{TPA}} = 1000$  GM at 750 nm and a fluorescence quantum yield of  $\phi \sim 0.87$  in THF. The two-photon activity decreased slightly (about 1.3 times) in toluene (non-polar solvent) and acetone (polar aprotic solvent), but it was substantially reduced (about 4.2 times) in polar protic solvents such as methanol. When **6** is processed to produce nanoparticles in highly polar protic media such as water, large two-photon activity is observed giving  $\delta_{\text{TPA}} = 514$  GM and  $\phi = 0.83$ . Furthermore, these nanoparticles exhibit good photostability. All these properties exhibited by aqueous suspensions of nanoparticles are attractive for possible applications, especially as fluorescent contrast agents utilized in fluorescence microscopy.

#### Acknowledgments

The authors thank Conacyt (Grants 83519 and 132946) and PAPPIT IN 214010 for financial support and CGSTIC-CINVESTAV and Xiuhcoatl cluster for calculation time. J. Rodríguez-Romero and

Jiménez-Sánchez thank CONACYT for PhD fellowships. The authors thank Martin Olmos for technical assistance, QFB. T. Cortez and Q. V. González for determination of NMR spectra and G. Cuéllar for HRMS spectra.

#### Appendix A. Supplementary data

Supplementary data related to this article can be found at <http://dx.doi.org/10.1016/j.dyepig.2012.12.029>.

#### References

- [1] Pawlicki M, Collins HA, Denning RG, Anderson HL. Two photon absorption and the design of two-photon dyes. *Angew Chem Int Ed* 2009;48:3244–66.
- [2] Belfield KD, Yao S, Bondar MV. Two-photon absorbing photonic materials: from fundamentals to applications. *Adv Polym Sci* 2008;213:97–156.
- [3] Kim HM, Jeong BH, Hyon JY, An MJ, Seo MS, Hong JH, et al. Two-photon fluorescent turn-on probe for lipid rafts in live cell and tissue. *J Am Chem Soc* 2008;130:4246–7.
- [4] Morel Y, Irimia A, Najechalski P, Kervella Y, Stephan O, Baldeck PL. Two-photon absorption and optical power limiting of bifluorene molecule. *J Chem Phys* 2001;114:5391–6.
- [5] Kawata S, Kawata Y. Three-dimensional optical data storage using photochromic materials. *Chem Rev* 2000;100:1777–88.
- [6] LaFratta CN, Fourkas JT, Baldacchini T, Farrer RA. Multiphoton fabrication. *Angew Chem Int Ed* 2007;46:6238–58.
- [7] Kim HM, Ehrlich JE, Heikal AA, Perry JW, Barlow S, Hu Z, et al. Structure–property relationships for two-photon absorbing chromophores: bis-donor diphenylpolyene and bis(styryl)benzene. *J Am Chem Soc* 2000;122:9500–10.
- [8] Albota M, Beljonne D, Brédas JL, Ehrlich JE, Fu JY, Heikal AA, et al. Design of organic molecules with large two-photon absorption cross sections. *Science* 1998;281:1653–6.
- [9] Mongin O, Porres L, Charlot M, Katan C, Blanchard-Desce M. Synthesis, fluorescence, and two-photon Absorption of a series of elongated rodlike and banana-shaped quadrupolar fluorophores: a comprehensive study of structure–property relationship. *Chem Eur J* 2007;13:1481–98.
- [10] Rumi M, Ehrlich JE, Heikal AA, Perry JW, Barlow S, Hu Z, et al. Structure–property relationships for two-photon absorbing chromophores: bis-donor diphenylpolyene and bis(styryl)benzene. *J Am Chem Soc* 2000;122:9500–10.
- [11] He GS, Tan LS, Zheng Q, Prasad PN. Multiphoton absorbing materials: molecular designs, characterizations and applications. *Chem Rev* 2008;108:1245–330.
- [12] Wang CK, Zhao K, Su Y, Ren Y, Zhao X, Luo Y. Solvent effects on the electronic structure of a newly synthesized two-photon polymerization initiator. *J Chem Phys* 2003;119:1208–13.
- [13] Nag A, Goswami D. Solvent effect on two-photon absorption and fluorescence of rhodamine dyes. *J Photochem Photobiol A: Chem* 2009;206:188–97.
- [14] Yan Y, Li B, Liu K, Dong Z, Wang X, Qian S. Enhanced two-photon absorption and ultrafast dynamics of a new multibranched chromophore with a dibenzothioephene core. *J Phys Chem A* 2007;111:4188–94.
- [15] Ma Z, Lu S, Fan QL, Qing CY, Wang YY, Wang P, et al. Syntheses, characterization, and energy transfer properties of benzothiadiazole-based hyperbranched polyfluorenes. *Polymer* 2006;47:7382–90.
- [16] Zhou H, Yang L, You W. Rational design of high performance conjugated polymers for organic solar cells. *Macromolecules* 2012;45:607–32.
- [17] Kucherak OA, Didier P, Mély Y, Klymchenko AS. Fluorene analogues of Prodan with superior fluorescence brightness and solvatochromism. *J Phys Chem Lett* 2010;1:616–20.
- [18] a) Zein S, Delbecq F, Simon D. A TD-DFT investigation of two-photon absorption of fluorene derivatives. *Phys Chem Chem Phys* 2009;11:694–702; b) Fitisil I, Fakis M, Polyzos I, Giannetas V, Persephonis P, Vellis P, et al. A two-

- photon absorption study of fluorene and carbazole derivatives. The role of the central core and the solvent polarity. *Chem Phys Lett* 2007;447:300–4.
- [19] Cheng YJ, Yang SH, Hsu CS. Synthesis of conjugated polymers for organic solar cell applications. *Chem Rev* 2009;109:5868–923.
- [20] Grimsdale AC, Chan KL, Martin RE, Jokisz PG, Holmes AB. Synthesis of light-emitting conjugated polymers for applications in electroluminescent devices. *Chem Rev* 2009;109:897–1091.
- [21] a) Chiang CL, Wu MF, Dai DC, Wen YS, Wang JK, Chen CT. Red-emitting fluorenes as efficient emitting hosts for non-doped, organic red-light-emitting diodes. *Adv Funct Mater* 2005;15:231–8;  
b) Usluer O, Demic S, Egbe DAM, Birckner E, Tozlu C, Pivrikas V, et al. Fluorene–Carbazole dendrimers: synthesis, thermal, photophysical and electro-luminescent device properties. *Adv Funct Mater* 2010;20:4152–61;  
c) Xing X, Zhang L, Liu R, Li S, Qu B, Chen Z, et al. A deep-blue emitter with electron transporting property to improve charge balance for organic light-emitting device. *ACS Appl Mater Interfaces* 2012;4:2877–80;  
d) Thangthong A, Prachumrak N, Namuangruk S, Jungstittiwong S, Keawin T, Sudyoasuk T, et al. Synthesis, properties and applications of biphenyls functionalized 9,9-bis(4-diphenylaminophenyl)fluorenes as bifunctional materials for organic electroluminescent devices. *Eur J Org Chem* 2012;27:5263–74.
- [22] Oar MA, Serin JM, Dichtel WR, Frechet JM. Photosensitization of singlet oxygen via two-photon-excited fluorescence resonance energy transfer in a water-soluble dendrimer. *Chem Mater* 2005;17:2267–75.
- [23] Chen CH, Hsu YC, Chou HH, Thomas KRJ, Lin JT, Hsu CP. Dipolar compounds containing fluorene and a heteroaromatic ring as the conjugating bridge for high-performance dye-sensitized solar cells. *Chem Eur J* 2010;16:3184–93.
- [24] Yao S, Ahn HY, Wang X, Fu J, Van Stryland EW, Hagan DJ, et al. Donor–acceptor–donor fluorene derivatives for two-photon fluorescence lysosomal imaging. *J Org Chem* 2010;75:3965–74.
- [25] Song S, Ju D, Li J, Li D, Wei Y, Dong C, et al. Synthesis and spectral characteristics of two novel intramolecular charge transfer fluorescent dyes. *Talanta* 2009;77:1707–14.
- [26] Homnick PJ, Lathi PM. Modular electron donor group tuning of frontier energy levels in diarylamino fluorenone push–pull molecules. *Phys Chem Chem Phys* 2012;14:11961–8.
- [27] Qin C, Islam A, Han L. Incorporating a stable fluorenone unit into D–A– $\pi$ –A organic dyes for dye-sensitized solar cells. *J Mater Chem* 2012;22:19236–43.
- [28] Lincker F, Delbosc N, Bailly S, Bettignies R, Billon M, Pron A, et al. Fluorenone-based molecules for bulk-heterojunction solar cells: synthesis, characterization, and photovoltaic properties. *Adv Funct Mater* 2008;18:3444–53.
- [29] Haid S, Marszalek M, Mishra A, Wielopolski M, Teuscher J, Moser JE, et al. Significant improvement of dye-sensitized solar cell performance by small structural modification in  $\pi$ -conjugated donor–acceptor dyes. *Adv Funct Mater* 2012;22:1291–302.
- [30] a) Omer KM, Ku SY, Wong KT, Bard AJ. Green electrogenerated chemiluminescence of highly fluorescent benzothiadiazole and derivatives. *J Am Chem Soc* 2009;131:10733–41;  
b) Li Y, Li BX, Tan WY, Liu Y, Zhu XH, Xie FY, et al. Structure-properties relationships in solution-processable single-material molecular emitters for efficient green organic light-emitting diodes. *Org Electron* 2012;13:1092–9.
- [31] a) Wang Y, Huang J, Zhou H, Ma G, Qian S, Zhu XH. Synthesis, optical properties and ultrafast dynamics of a 2,1,3-benzothiadiazole-based red emitter with intense fluorescence and large two-photon absorption cross-section. *Dyes Pigm* 2011;92:573–9;  
b) Kato SI, Matsumoto T, Shigeiwa M, Gorohmaru H, Maeda S, Ishi-I T, et al. Novel 2,1,3-benzothiadiazole-based red-fluorescent dyes with enhancement two-photon absorption cross-section. *Chem Eur J* 2006;12:2303–17.
- [32] Liu SJ, Zhao Q, Chen RF, Deng Y, Fan QL, Li FY, et al.  $\pi$ -Conjugated chelating polymers with charger iridium complexes in the backbones: synthesis, characterization, energy transfer, and electrochemical properties. *Chem Eur J* 2006;12:4351–61.
- [33] Liu L, Wong WY, Lam YW, Tam WY. Exploring a series of monoethynyl-fluorenes as alkynylating reagents for mercuric ion: synthesis, spectroscopy, photophysics and potential use in mercury speciation. *Inorg Chim Acta* 2007;360:109–21.
- [34] Khan MS, Al-Mandhary MRA, Al-Suti MK, Ahrens B, Mahon MF, Male L, et al. Synthesis, characterization and optical spectroscopy of diynes and poly-yne containing derivatised fluorenes in the backbone. *Dalton Trans* 2003:74–84.
- [35] Mello JC, Wittmann F, Friend RH. An improved determination of external photoluminescence quantum efficiency. *Adv Mater* 1997;9:230–2.
- [36] Xu C, Webb WW. Measurement of two-photon excitation cross sections of molecular fluorophores with data from 690 to 1050 nm. *J Opt Soc Am B* 1996;13:481–91.
- [37] Makarov NS, Drobizhev M, Rebane A. Two-photon absorption standards in the 550–1600 nm excitation wavelength range. *Opt Express* 2008;16:4029–47.
- [38] Wang XH, West DP, McKeown NB, King TA. Determining the cubic susceptibility (3) of films or glasses by the Maker fringe method: a representative study of spin-coated films of copper phthalocyanine derivation. *J Opt Soc Am B* 1998;15:1895–903.
- [39] Muñoz BM, Santillan R, Rodríguez M, Méndez JM, Romero M, Farfán N, et al. Synthesis, crystal structure and non-linear optical properties of boronates derivatives of salicylideneiminophenols. *J Organomet Chem* 2008;693:1321–34.
- [40] Komáromi A, Tolnai GL, Novák Z. Copper-free Sonogashira coupling in amine–water solvent mixtures. *Tetrahedron Lett* 2008;49:7294–8.
- [41] Park KK, Tsou LK, Hamilton AD. Facile and selective aerobic oxidation of arylalkanes to aryl ketones using cesium carbonate. *Synthesis* 2006;3617–20.
- [42] Neto BAD, SantAna-Lopes A, Ebeling G, Gonçalves RS, Costa VEU, Quina FH, et al. Photophysical and electrochemical properties of  $\pi$ -extended molecular 2,1,3-benzothiadiazoles. *Tetrahedron* 2005;61:10975–82.
- [43] Ouyang X, Huo Y, Lu L, Ge Z, Ji W. Observation of tunable two-photon induced excited-state and three-photon absorption phenomena by structure in oligomerfluorene derivatives. *Appl Phys A-Mater* 2011;105:891–5.
- [44] Rodrigues PC, Berlim LS, Azevedo D, Saavedra NC, Prasad PN, Schreiner WH, et al. Electronic structure and optical properties of an alternated fluorene–benzothiadiazole copolymer: Interplay between experimental and theoretical data. *J Phys Chem A* 2012;116:3681–90.
- [45] Lincker F, Heinrich B, Bettignies R, Rannou P, Pécaut J, Grévin B, et al. Fluorene core donor–acceptor–donor  $\pi$ -conjugated molecules end-capped with dendritic oligo(thiophene)s: synthesis, liquid crystalline behavior, and photovoltaic applications. *J Mater Chem* 2011;21:5238–47.
- [46] Roquet S, Cravino A, Leriche P, Aleveque O, Frere P, Roncali J. Triphenylamine-thienylenevinylene hybrid systems with internal charge transfer as donor materials for heterojunction solar cells. *J Am Chem Soc* 2006;128:3459–66.
- [47] Lakowicz JR. Principles of fluorescence spectroscopy. 3rd ed. Singapore: Springer; 2006.
- [48] Reichardt C. Solvents and solvent effects in organic chemistry. 3rd ed. Weinheim: Wiley-VCH; 2003. 1 reprint 2004.
- [49] Farcas A, Jarroux N, Harabagiu V, Guégan P. Synthesis and characterization of a poly[2,7-(9,9-dioctylfluorene-alt-2,7-fluorene/ $\beta$ -CD)] main chain polyrotaxane. *Eur Polym J* 2009;45:795–803.
- [50] Peng Q, Lu ZY, Huang Y, Xie MG, Han SH, Peng JB, et al. Synthesis and characterization of new red-emitting polyfluorene derivatives containing electron deficient 2-pyran-4-ylidene-malonitrile moieties. *Macromolecules* 2004;37:260–6.
- [51] Luo J, Yang R, Yang W, Cao Y. Optoelectronic properties of fluorene-co-4,7-difuran-2,1,3-benzothiadiazole copolymers. *Sci China Chem* 2010;53:576–80.
- [52] Saroja G, Soujanya T, Ramachandram B, Samanta A. 4-Aminophthalimide derivatives as environment-sensitive probes. *J Fluorescence* 1998;8:405–10.
- [53] Fery-Forgues S, Fayet JP, Lopez A. Drastic changes in the fluorescence properties of NBD probes with the polarity of the medium: involvement of a TICT state. *J Photochem Photobiol A: Chem* 1993;70:229–43.
- [54] a) Lippert Von E. Spektroskopische bestimmung des dipolmomentes aromatischer verbindungen im ersten angeregten singulettzustand. *Z Electrochem* 1957;61:962–75;  
b) Mataga N, Kaifu Y, Koizumi M. Solvent effects upon fluorescence spectra and the dipole moments of excited molecules. *Bull Chem Soc Jpn* 1956;29:465–70.
- [55] Onsager L. Electric moments of molecules in liquids. *J Am Chem Soc* 1936;58:1486–93.
- [56] Baathulaa K, Xu Y, Qian X. Unusual large Stokes shift and solvatochromic fluorescence: synthesis, spectra, and solvent effect of 6-substituted 2,3-naphthalimide. *J Photochem Photobiol A: Chem* 2010;216:24–34.
- [57] Fung SY, Duhamel J, Chen P. Solvent effect on the photophysical properties of the anticancer agent ellipticine. *J Phys Chem A* 2006;110:11446–54.
- [58] Frisch MJ, Trucks GW, Schlegel HB, Scuseria GE, Robb MA, Cheeseman JR, et al. Gaussian 03, revision B.01. Wallingford, CT: Gaussian, Inc.; 2004.
- [59] a) Utinans M, Neilands O. Quantum chemical calculations, synthesis and properties of novel organic molecules with photoinduced intramolecular electron transfer and large change in electric dipole moment in the excited state. *Adv Mater Opt Electron* 1999;9:19–25;  
b) Gong Y, Guo X, Wang S, Su H, Xia A, He Q, et al. Photophysical properties of photoactive molecules with conjugated push–pull structures. *J Phys Chem A* 2007;111:5806–12.
- [60] Nalwa HS, Kakuta A, Mukoh A, Kasai H, Okada S, Oikawa H, et al. Fabrication of organic nanocrystals for electronics and photonics. *Adv Mater* 1993;5:758–60.
- [61] Ramos-Ortiz G, Maldonado JL, Hernández MCG, Zolotukhin MG, Fomine S, Fröhlich N, et al. Synthesis, characterization and third-order non-linear optical properties of novel fluorene monomers and their cross-conjugated polymers. *Polymer* 2010;51:2351–9.
- [62] Cheng JZ, Lin CC, Chou PT, Chaskar A, Wong KT. Fluorene as the  $\pi$ -spacer for a new two-photon absorption chromophores. *Tetrahedron* 2011;67:734–9.
- [63] Lin TC, Lee YH, Huang BR, Hu CL, Li YK. Two-photon absorption and effective optical power-limiting properties of small dendritic chromophores derived from functionalized fluorene/oxadiazole units. *Tetrahedron* 2012;68:4935–49.